Cross-Sectional Scanning Tunneling Microscopy Applied to Complex Oxide Interfaces

*Te Yu Chien, Jak Chakhalian, John W. Freeland, and Nathan P. Guisinger**

Understanding interfacial science is critical to many modern technologies. It is very common in solid-state physics for electronic properties to show novel phenomena when combining various dissimilar materials at atomically abrupt interfaces. For example, semiconductor interfaces have provided the foundation of modern electronic devices for several decades. Now with advances in growth and synthesis, controllable high quality complex oxide heterojunctions can be routinely fabricated. Since complex oxide materials exhibit a wide variety of functionalities owing to their strong coupling to the electron, lattice, orbital and spin degrees of freedom, these materials display a wide spectrum of interesting functionalities. Combining dissimilar complex oxides at interfaces allows one to explore and create intriguing phenomena that are not attainable in the lone bulk constituents. However, the key challenge has been the direct characterization of these interfaces at the nanoscale in order to understand the physical properties found at complex oxide interfaces. This requires the development of new experimental approaches. In this paper, we review the utilization of cross-sectional scanning tunneling microscopy/spectroscopy as a *direct probe* of these oxide interfaces at the nanoscale. This technique provides valuable insight to both structural and electronic properties of these unique systems and enables understanding of the detailed electronic structure (e.g., local electronic density of states (LDOS), charge transfer, band bending, etc.) at oxide interfaces, which is of key interest to both fundamental and applied science.

1. Introduction

Cross-sectional scanning tunneling microscopy (XSTM) is a powerful tool that has been utilized for characterizing several unique material systems. This technique has traditionally been applied to compound semiconductors (GaAs, InAs, etc.) that have natural cleavage planes.[1–5] These materials are cleaved in situ and generally yield very high quality surfaces with extremely large atomic terraces. Studies have included basic investigation of the bulk material properties, dopants within the material, and recently the study of magnetic impurities and their role in dilute magnetic semiconductors.[6–9] Moreover, this technique has gone beyond characterizing the bulk properties of the material and has been applied to buried semiconductor heterostructures.[10–20] In recent years, more technically advanced techniques have utilized XSTM to encapsulate and fracture semiconductor nanowires to study their cross-section at the atomic scale.[21–23] XSTM has also been applied to high-temperature superconducting materials that have natural cleavage planes and has been instrumental in exploring superconductivity and the electronic properties of these materials.[24–33] The novel element of our approach is to apply XSTM to complex oxide materials and heterostructures that "do not" have a natural cleavage plane. In other words, by virtue of fracturing (not cleaving) our samples in situ, we demonstrate that even under these conditions, we can readily find regions of atomically flat surfaces sufficient for XSTM studies.

Dr. T. Y. Chien, Dr. J. W. Freeland
Advanced Photon Source
Argonne National Laboratory
Argonne, IL 60439, USA
Prof. J. Chakhalian
Department of Physics
University of Arkansas
Fayetteville, AR 72701, USA
Dr. N. P. Guisinger
Center for Nanoscale Materials
Argonne National Laboratory
Argonne, IL 60439, USA
E-mail: nguisinger@anl.gov

DOI: 10.1002/adfm.201203430

1.1. Why Complex Oxides?

Recently complex oxide interfaces with strong electron correlations have been at the forefront of materials science, owing largely to the fact that traditional semiconductor physics is not capable of fully describing the underlying physics of these materials and a new framework is needed.[34–36] Great varieties of functionalities have been discovered in this class of materials. For example, colossal magnetoresistance (CMR),[37] high Tc superconductivity (SC),[38] ferroelectricity (FE),[39–41] and multiferroics (MF)[42] have all been observed in oxide-based compounds. The ultimate goal is to utilize the unique physical properties of this class of materials, such as metal-to-insulator transitions, superconductivity, and magnetism, to either optimize existing devices or develop new commercial applications. One of the key challenges towards understanding a material's macroscopic behavior (e.g., CMR, SC, and MF) typically involves a thorough exploration and understanding at the smallest possible length-scales.

In a two-dimensional (2D) environment, such as at surfaces, structural,[43] electronic,[44] spin,[45,46] and orbital[47]

reconstructions have been observed due to the broken symmetries. Not surprising, these reconstructions (charge,[34] spin,[48] lattice,[49] and orbital)[50] have also been observed at interfaces, which also have broken translational symmetry in addition to the altered chemical environment. With the aforementioned variety of functionalities found in complex oxides, the emerging phenomena at the complex oxide interfaces have exhibited interesting possibilities for potential new technologies.[51] However, the search for next generation electronic devices will depend on the understanding and further controlling the behavior at interfaces in complex oxide materials.[52,53] Many experimental tools have been used to probe the physical properties at the proximity of interfaces, but what is needed to further understand oxide interfaces is a tool with excellent spatial resolution as well as the ability to extract physical properties. This is why scanning probe microscopies are ideal characterization tools that offer the potential to gather new information at the nano and atomic scale.

2. Transition Metal Oxides Interfaces and Probing Techniques

2.1. Complex Oxides: Perovskites

Conventionally, complex oxides refer to the transition metal oxide materials with strong electron correlation and coupling interactions. These materials are found to naturally form several different crystal structures, including wurzite, spinel, anatase, fluorite, and perovskites.[52] This paper is solely focused on oxides that have a perovskite crystal structure, but it should be noted that the proposed approach is certainly not limited to this class of crystals. The structure of a simple perovskite (ABO_3) in the (001) direction is composed of an alternate stacking of BO_2, and AO layers, as illustrated in the crystal schematic of **Figure 1**a. The same ABO_3 crystal structure can exhibit numerous functionalities by merely substituting elements at the A and B sites. For example, CMR effects are observed in manganese-based perovskite oxides ($La_{1-x}Ca_xMnO_3$ or $La_{1-x}Sr_xMnO_3$),[37] while FE can be seen in titanium-based oxides,[39–41] and MF in $BiFeO_3$.[42] Due to the similar structure and lattice constant among different perovskites, high quality epitaxial thin film growth has been proven successfully on a variety of perovskite substrates, as illustrated in the crystal schematic of Figure 1b, of which $SrTiO_3$ (STO) is one of the most common substrates.[54]

One of the most interesting phenomena observed in oxide materials involves the observations of new material properties that are not intrinsic to the individual constituents. For instance, a high mobility electron gas and superconductivity has been reported at the interface of two band insulators–$LaAlO_3/SrTiO_3$ (LAO/STO);[55,56] spin rearrangement and orbital reconstruction at the interfaces of superconductor and ferromagnetic material–$YBa_3Cu_2O_7/La_{2/3}Ca_{1/3}MnO_3$;[48,50] superconductivity at the interfaces of insulating and metallic phases of cuprates–$La_2CuO_4/La_{1.56}Sr_{0.45}CuO_4$;[57] ferromagnetism (FM) at the interfaces of two anti-ferromagnetic (AFM) materials–$LaFeO_3/LaCrO_3$[58] and at the interfaces between an AFM insulator and a paramagnetic metal–$CaMnO_3/CaRuO_3$;[59] AFM coupling between layers of FM materials–$La_{0.7}Sr_{0.3}MnO_3/SrRuO_3$;[60] and multiferroic phase generated by combining FE and FM materials–$BiFeO_3/CoFe_2O_4$.[61] One of the important factors that affect the properties at interfaces is how the interface is terminated. More specifically, when another perovskite, $A'B'O_3$, grown on it, the interface can be either terminated with $A'O/BO_2$ or $B'O_2/AO$ sequence. For example, Figure 1b shows the $B'O_2/AO$ terminated interface. Such stacking of the atomic planes can have a large influence on the interface properties as noted by the example of an 2D electron gas (2DEG) observed at LAO/STO interfaces; the 2DEG only appears when more than three unit cells of LAO are grown on TiO_2 terminated STO surfaces, but not on SrO terminated STO surfaces at all.[55]

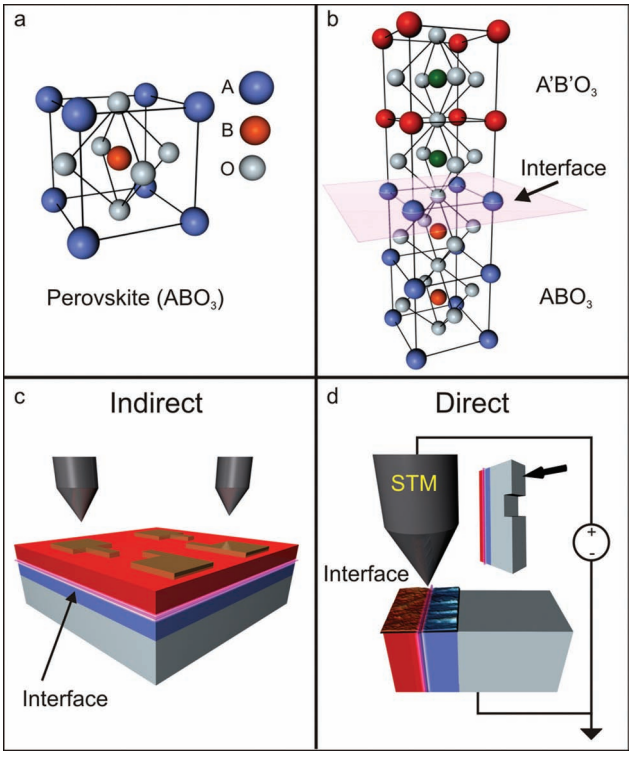

Figure 1. a) Atomic arrangement in the unit cell of ABO_3 perovskite. b) Atomic arrangement in the proximity of the interface with $B'O_2/AO$ stacking sequence. The interface layer is highlighted with light-pink plane. c) Schematic of indirect method probing the buried interface properties. d) Schematic of XSTM/S probes interfaces directly. The inset illustrates the pre-notched fracturing for XSTM/S studies.

2.2. Challenge: Characterization of Electronically Active Buried Oxide Interfaces

One of the primary techniques for characterizing the functionality of oxide heterostructures involves macroscopic transport techniques, where large contacts are patterned on the topmost layer, as illustrated by the schematic in Figure 1c. The transport measurements reveal the fascinating physics reported on these systems as a whole but are clearly an indirect method for probing interfacial science. Of the common techniques

used for probing interfaces, only a few have the capability of nanoscale spatial resolution while directly extracting electronic, chemical or physical properties. One of the leading techniques is high-resolution cross-sectional transmission electron microscopy (HR-XTEM), but this technique is limited in its ability to extract the local density of state (LDOS) near Fermi energy that dictates the measured transport properties.[62] In contrast, scanning probe microscopy (SPM) can provide excellent spatial resolution while directly probe the local behavior of electrons close to the Fermi level.

To date, SPM techniques have been primarily utilized to characterize surface properties of oxide thin films or the substrate with very little application towards direct characterization of oxide interfaces, as shown in Figure 1c. For instance, STM combined with spectroscopy techniques (scanning tunneling spectroscopy–STM/S) has been applied to study surface reconstructions and various surface properties for many clean complex oxide surfaces prepared in situ under ultrahigh vacuum (UHV).[63–65] Also recently, the conducting atomic force microscopy (cAFM) was used to control (write and erase) the conductivity at LAO(3 unit cell)/STO(TiO_2 terminated) interfaces in an ambient environment.[66]

One of the first applications to directly probe an oxide interface with SPM was achieved by Basletic et al. where they recently reported a clear cAFM mapping in cross-sectional view of LAO/STO interfaces, revealing the direct evidence of the existence of the highly conductive interface.[67] The reported method of preparing the cross-sectional view of the LAO/STO interfaces is by gluing two films together followed by mechanical polishing. However, this method is not suitable for STM/S measurements due to the rough surface caused by the detrimental mechanical polishing procedure. Since STM/S could provide information related to elecronic LDOS, in order to further understand the band interaction between dissimilar materials at interfaces, a procedure of creating the most pristine cross-sectional view is needed.

2.3. Solution: In Situ Fracturing of Complex Oxides

In an effort to utilize the atomic-resolution of the STM and STS towards directly probing oxide interfaces, an ideal approach would be to apply the concepts of XSTM to oxide materials and heterostructures. However, since perovskites do not have a natural cleavage plane, we need to develop a technique that is technically fracturing the material, but, if successful, would enable the ability to directly probe pristine interfaces that have not been subjected to any additional processing.

Based on this motivation, we have successfully developed a *controllable* fracturing method to create a ready-to-scan cross-sectional view for the complex oxide interfaces by STM.[68–70] As previously mentioned, the first challenge is to fracture oxide materials that do not possess a natural cleavage plane. For example, when a shear force or a tensile force is applied to the material with a natural cleavage plane along the in-plane or the out-of-plane directions, the material will cleave at certain atomic layers (i.e., the cleavage planes) resulting in atomically flat surfaces. As a consequence, it is not surprising that there are numerous STM studies investigating the surfaces of layered oxides.[71–73] In sharp contrast, for ABO_3, since there is no relative strong/weak bonding in the structure, no natural cleavage planes exist. When these materials are subjected to a shear force, the perovskite will "fracture" with macroscopic roughness, similar to the morphology seen for fractured glass.[68] However, since relatively few SPM studies exist for fractured ABO_3 perovskites.[68–70,74–76] and a microscopic understanding of the fractured ABO_3 perovskite's surface is still unclear. Since our initial focus was perovskites, it was necessary to develop a controllable fracturing technique in order to reliably prepare complex oxide specimens for XSTM/S characterization.

The controlled fracturing method is based on the creation of a notch to nucleate the initial crack formation. First, we scribe the samples by using precision dicing saw to create the notch. The sample thickness is typically 1 mm or 0.5 mm for the studies involving Nb-doped $SrTiO_3$ (Nb:STO) substrates.[68–70,76] The scribing depth was controlled within a range from 50% to 70% of the sample thickness. Then the fracturing was performed in situ prior to the STM/S measurements under ultrahigh vacuum (UHV) environment, as illustrated in Figure 1d.[68–70,76] For increased quality and control, samples are mounted rigidly with a set of clamps where the notch is aligned to the top surface of the clamps. The samples are fractured in situ by moving the mounted samples against a rigid cleaver in the UHV chamber. By doing this controlled fracturing process at room temperature (RT), the fractured Nb:STO surfaces exhibit micrometer roughness macroscopically but display well defined atomic planes with low atomic roughness at the nanoscale.[68]

3. XSTM/S Applied to Fractured Complex Oxides

3.1. Bulk Nb-Doped $SrTiO_3$: Alternating Striped Surface Terminations

Nb:STO was the first example for the application of the XSTM/S. The choice of Nb:STO is due to the fact that STO is a very common substrate material and the Nb-doping induces a metallic state with adequate conductivity for STM imaging. It is known that the morphology of the glass surfaces after fracturing is composed of a few distinct types of regions: mirror, mist, hackle, and conchoidal lines.[77] The fractured Nb:STO morphology revealed by scanning electron microscopy (SEM) shows similar features as that of the fractured glass.[68] With the morphology established by SEM, the main question becomes: "can we image these fractured samples that are macroscopically rough with a nanoscale probe?" In order to answer this question, we performed STM studies on the fractured Nb:STO surfaces.[68–70,76] It was found that we can readily find atomically flat regions with relatively large terraces, as illustrated in the representative STM image of **Figure 2**a.

The schematic inset shown in the left panel of Figure 2a illustrates the SrO/TiO_2 stacking sequence in bulk STO. Since this material does not have a cleavage plane, by symmetry we expect an equal mixture of SrO and TiO_2 termination on the surface. To our surprise, the fractured Nb:STO surfaces does in fact have a roughly 50:50 mixed surface terminations, but, rather than

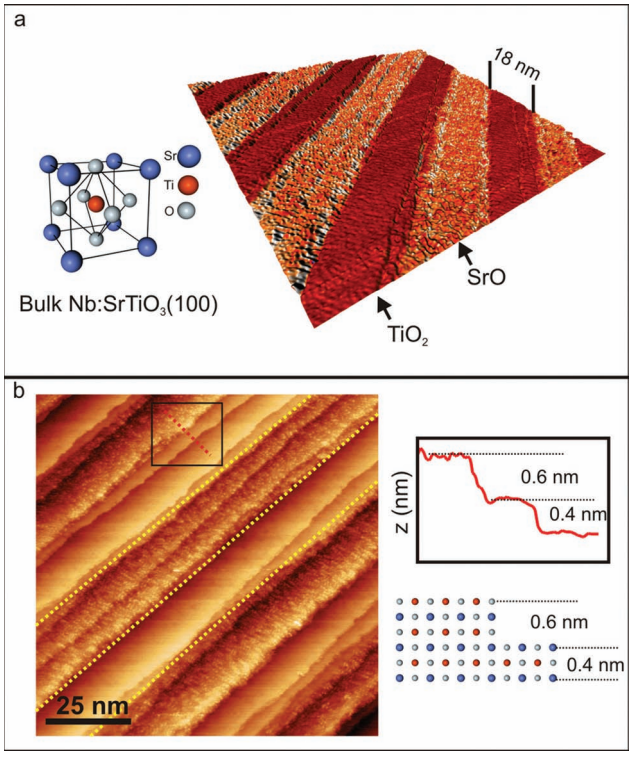

Figure 2. a) Long-range stripes observed on the Nb:STO surfaces after the controlled fracturing. The inset shows the unit cell. b) Left panel shows the morphology of the stripes pattern. Rough and smooth morphologies appear alternatively. Right panel shows the line profile indicated in the black square/red dashed line in the left panel. The height change was found to be 0.6 nm (1.5 lattice constant) when crossing different types of morphology; while it was 0.4 nm (1 lattice constant) when crossing the step within the same type of morphology.

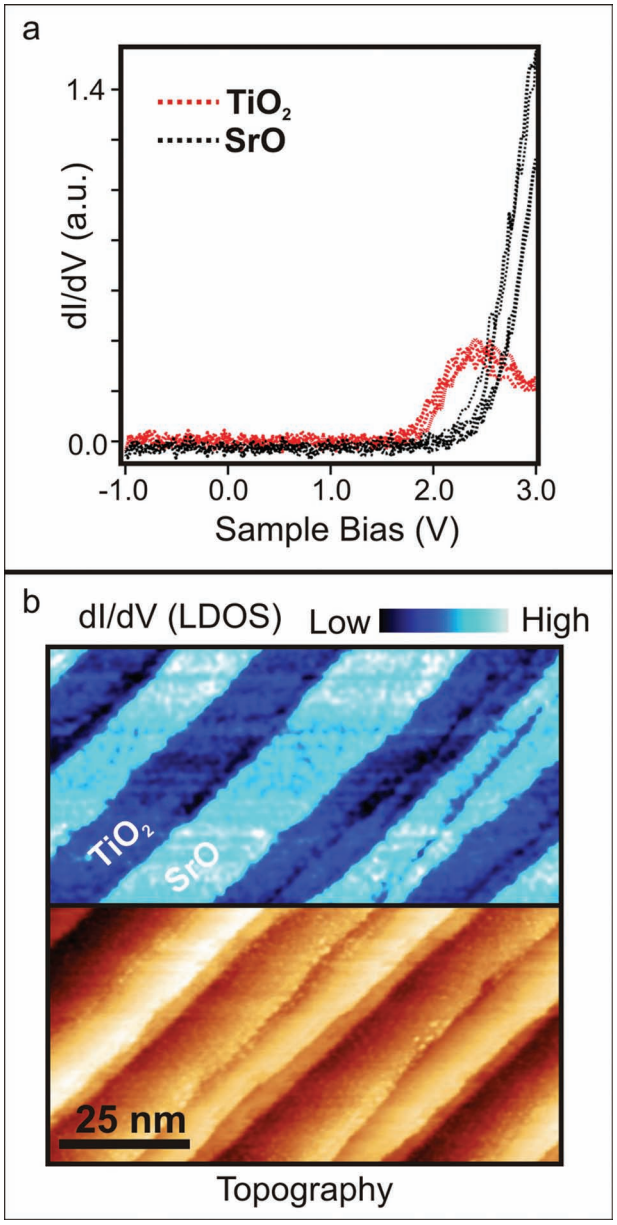

Figure 3. a) *dI/dV* spectra measured at the two regions with distinct morphologies. The rough regions (black lines) are assigned to SrO terminated surfaces; while the smooth regions (red lines) are assigned to TiO_2 terminated surfaces. b) *dI/dV* contrast (top) and topography (bottom) measured at 3.0 V simultaneously on the fractured Nb:STO surfaces.

being random, the terminations form alternating long-range striped patterns,[69] as shown in the STM images of Figure 2a,b. These two types of surface termination have very distinct morphologies (roughnesses of 0.2 nm and 0.05 nm), which is clearly evident in the STM image of Figure 2b.[69] Furthermore, the step heights are half-integer unit cell (0.2 nm or 0.6 nm) when crossing the borders between the rough and smooth regions while the step heights within the same termination region are integer unit cell in size (see topographic line scan in Figure 2b). In short, from the topographic data alone, we observe a change in morphology that is half of a unit cell suggesting a change in surface termination, as illustrated in the schematic model following the line scan at the bottom right of Figure 2b.

To further explore the striped surface patterns that appear to be an ordered pattern of surface terminations, the utilization of STS was implemented to probe the LDOS, which is proportional to the *dI/dV* signal. The *dI/dV* signal is measured with a lock-in amplifier while a small *ac* modulation is added to the constant *dc* bias voltage applied between tip and sample. This technique can be utilized to measure the conductance as a function of energy and can also be used concurrently with topographic imaging to spatially map the conductance at one particular energy (tip-sample bias). Furthermore, by sweeping the tip-sample bias, the LDOS as function of energy near the Fermi level can be revealed. As shown in **Figure 3**a, two distinct spectra were recorded in the morphologically rough and smooth regions. Under negative bias (occupied states), both terminations show negligible LDOS due to the large spacing between the Fermi level and the valence band edge, which is not in the measured bias region. On the other hand, under positive bias (unoccupied states), the smooth regions show a higher LDOS between ~1.8–2.4 V. By comparing with DFT calculations of the electronic structure vs surface termination,[78,79] the rough and the smooth regions are assigned to SrO and TiO_2 terminated surfaces, respectively, as indicated in Figure 3a. Figure 3b

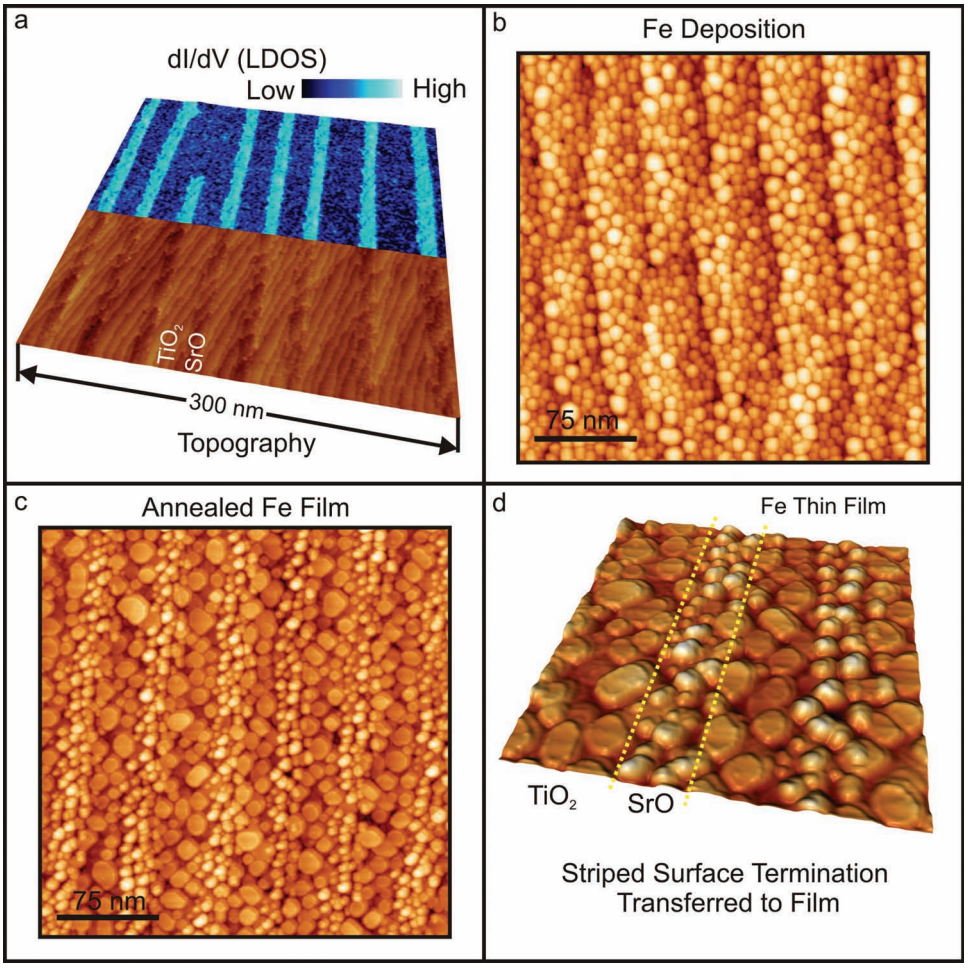

Figure 4. a) The dual-terminated stripes pattern on Nb:STO right after the controlled fracturing. b) As-deposited Fe film on the fractured Nb:STO. c) the morphology of the Fe film after 650 °C, 10 min annealing. d) the 3D image of c), showing dot-like and plateau-like morphology in two regions.

shows the *dI/dV* conductance measured at +3.0 V sample bias along with the topography recorded simultaneously. At this particular energy, it is clear that the SrO terminated regions have a higher *dI/dV* contrast, consistent with the *dI/dV* spectra shown in Figure 3a.

The microscopic origin of the stripe pattern is still unclear but is certainly a result of the fracturing process. The interesting aspect is that we always observe alternating striped surface terminations when fracturing at RT. In addition, for rougher fractures, it is clearly observed that the striped segregation is not connected to the orientation of resulting step-edges. Future work including experiments to monitor the fracture direction vs. the stripe orientation is needed to fully understand the fracture dynamics.

3.2. Surface Termination Pattern Transfer to Thin Films

Since the termination at the interfaces is a critical factor affecting the interface properties or even the properties of subsequently grown films, in this section we explore how the striped alternating surface terminations can be used as a template for controlling the morphology of thin film growth. In this direction, the striped fractured Nb:STO surfaces were used to investigate the influence of the surface termination on deposited Fe films.[80] First, we prepared a dual terminated striped pattern on the fractured Nb:STO as illustrated in the STM image of **Figure 4**a. The widths of the TiO_2 and SrO terminated regions are 25 nm and 10 nm, respectively.

Fe was then deposited on the fractured Nb:STO surfaces at room temperature using e-beam evaporation. The as-deposited Fe films exhibited a complex nanoscale morphology with average dot size/separation to be around 3.7 ± 1.0 nm (Figure 4b).[80] Although the steps are still somewhat visible, there is no discernable difference of Fe islands on regions of different surface termination. However, upon annealing at 650 °C for 10 min, the Fe film morphology separates dramatically into two distinct regions; dot-like morphology similar to the original dots of the as deposited films, but larger (~8 nm in diameter), and regions in which the Fe develops larger plateau-like islands, as shown in the STM images of Figure 4c,d. Though the scanning regions before and after Fe deposition cannot be exactly the same, using the starting images we can assign the dot-like region and the plateau-like regions to Fe/SrO and Fe/TiO_2 regions, respectively.

The change of film morphology upon annealing is driven by the competition between the surface energy and the energy at Fe/SrO or Fe/TiO_2 interfaces.[80] Before annealing, the surface energy of the Fe film is identical everywhere because the morphology of Fe films is identical over the entire scanning area. Upon annealing, the Fe dots evolve depending on the distinct interfacial energy at Fe/SrO and Fe/TiO_2 interfaces. It is well known that the SrO regions has a rougher morphology due to vacancies and adatoms within this surface termination, which is not nearly as stable as the TiO_2 termination. This in turn means that the SrO is morphologically rougher and also has reactive dangling bonds. The overall surface energy of this region is higher than that of the TiO_2; the higher surface energy minimizes Fe diffusion and restricts coalescence. Hence, the regions of Fe deposition on SrO look fairly unchanged but only the sizes of the dots increased after temperature processing. In contrast, the smooth and structurally robust TiO_2 regions have a lower surface energy, which allows Fe to diffuse more easily and coalesce into larger single crystal islands.

3.3. Controlled Modification of the Surface Termination

The sample temperature during fracture can also be utilized to control the resulting fractured surfaces. Large terraces (~500 nm in width) can be achieved by fracturing Nb:STO at ~55 K, as shown in **Figure 5**a.[76] One possible explanation is that the low temperature fracture will reduce the appearance of the steps, which could be considered as a planar type of defects on fractured surfaces. Similar temperature dependent cleaving behavior was revealed for layered perovskites. Pennec et al. compared two Sr_2RuO_4 samples fractured at 20 K and 200 K and showed that the sample fractured at 20 K shows much smaller defect density due to decreased SrO mobility on the surface.[71] Another possible reason is that the fracturing behavior of Nb:STO at 55 K is different from that at RT due to the temperature dependent structural phase transition. STO goes through phase transition at ~105 K from a high temperature cubic phase ($Pm\ \bar{3}m$ (O^1_h)) to a low temperature tetragonal phase ($I4/mcm$ (D^{18}_{4h})).[81] A closer examination of the large terrace showed the roughness was ~0.2 nm, which is similar to the SrO terminated surfaces on the RT fractured Nb:STO. Based on the magnitude of roughness, it is believed that the low temperature fractured surfaces contain a 50% incomplete SrO reconstruction with a high density of randomly distributed vacancies/adatoms distributed over a complete TiO_2 termination, and so for the other side of the fractured specimen (the one broken off and at the bottom of the chamber), as illustrated in Figure 5b. This view is supported by atomic resolution images showing random clusters on an atomically flat surface (not shown).[76]

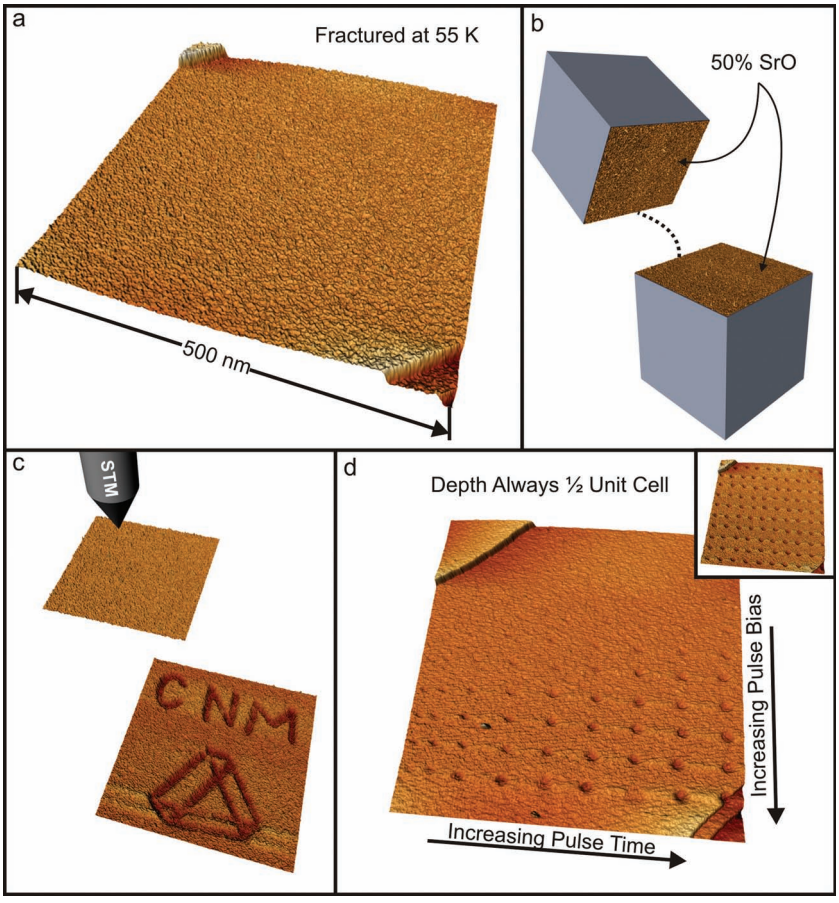

Figure 5. a) Large terrace created by low temperature (LT) (~55 K) fracturing. b) Schematic of the possible 50% SrO random clusters on the LT-fractured Nb:STO surfaces. c) Nano-lithography on the LT-fractured Nb:STO surfaces with STM tip. d) The demonstration how tip-sample bias and duration control the lateral sizes of the hole created by the nano-lithography. The inset shows one hundred holes created by the identical condition, revealing the controllability.

We also found that this incomplete SrO termination can be manipulated by the strength of the electric field applied at the tip-sample junction, which provides a means of controlled manipulation of the surface termination at the nanoscale.[76] Figure 5c shows a pattern created by STM tip lithography on the low temperature fractured surface of Nb:STO. The STM nano-patterning can be controlled by a variety of factors including the tip-sample bias and duration over which it is applied. With a set point of 1.4 V and 50 pA for imaging only, the ability for the tip to manipulate the surface as a function of bias voltage pulse magnitude (positive) and pulse duration is shown in Figure 5d.[76] The depths of the holes created by the electric pulse method are mostly 0.2 nm, which is half integer unit-cell height, despite the bias and duration. This indicates that the SrO clusters are removed either onto the tip or away from the imaging region.[76] The change of the dI/dV contract in the hole is consistent with exposure of the underlying TiO_2 terminated surface.[76] With the same tip, at least one hundred identical holes could be created by electric pulses with same bias and duration, as shown in the inset of Figure 5d illustrating the potential use as a nano-lithographic method.

In addition to the positive bias manipulation (hole creation), a negative bias can re-deposit the SrO clusters from the tip back to the desired locations on the surfaces.[76] In fact, the re-deposition from tip to sample with negative bias could be performed at any location on the surface, even in the hole created by positive bias. Negative bias pulsing induced re-deposition is also confirmed by the observation that the fresh tip, which does not have any SrO adsorbate, is not able to deposit clusters and a clean tip could be achieved by a negative bias pulsing procedure.[76] In other words, the tip can be conditioned and cleaned by the negative bias pulses after scanning degrades the tip condition. For experiments aiming to probe interfaces in cross-section, this information is valuable since the finding the interface often requires significant scanning and large distance moves, which can degrade the tip.

4. Interfaces

4.1. Manganites: $La_{2/3}Ca_{1/3}MnO_3$ - Nb:$SrTiO_3$

In this section, we describe the first successful XSTM/S measurement on a perovskite complex oxide interface, which we achieved on the $La_{2/3}Ca_{1/3}MnO_3$/Nb-doped $SrTiO_3$ (LCMO/Nb:STO) system.[82] The sample preparation used in this study is based on the controlled fracturing process described above. One of the challenges for achieving smooth regions at the interface, which is also close to the edge of the substrate, is to control the fracturing direction. Since the fracturing is accomplished by introducing a bending strain by pushing the scribed samples against a rigid cleaver, the fulcrum side of the sample can be severely damaged. In other words, the film/interface side of the sample cannot be placed on the fulcrum side. On the other hand, if the film/interface is placed on the initial cracking side, the fracture near the interface is not reliable due to the lack of initial weak notch. After several attempts, we found that the best way to fracture the sample is to scribe the sample from the side, which damages part of the film, but leaves the rest of the film intact. Then fracture the sample from the notch side. By doing so, the films are more consistent with less damage and have well-defined interfaces for XSTM/S measurements.

Another issue is finding the interface with STM tip. This problem could be resolved by having a scanning electron microscopy (SEM) in the STM system, so that the tip position could be easily manipulated to land on the region near or right on interfaces. However, without having a SEM in STM system, the STM tip can only land on the fractured surfaces without knowing the exact distance to the interface. When "walking" toward the interface, the tip speed should be kept slow while having the constant current feedback loop on. In the case of Nb:STO, we typically used a set point of +3.0 V and 50 pA with a cruise speed set at 100 nm/s. Furthermore, the tip degradation issue due to tip-sample interaction is unavoidable during this long walking/searching procedure. As suggested above, negative bias pulses are essential for reconditioning the tip after locating the interfaces

Figure 6a illustrates a possible atomic arrangement at the LCMO/Nb:STO interface and Figure 6b shows a falsely colored topographic XSTM image of the fractured LCMO/Nb:STO interface. In the Nb:STO region, the dual-terminated surfaces, that were observed previously on the fracture surfaces of Nb:STO (see Section 3.1), extends all the way to the interface, as seen in Figure 6b and the zoom-in view in **Figure 7**a; notice, the *dI/dV* contrast can be used to distinguish SrO and TiO_2

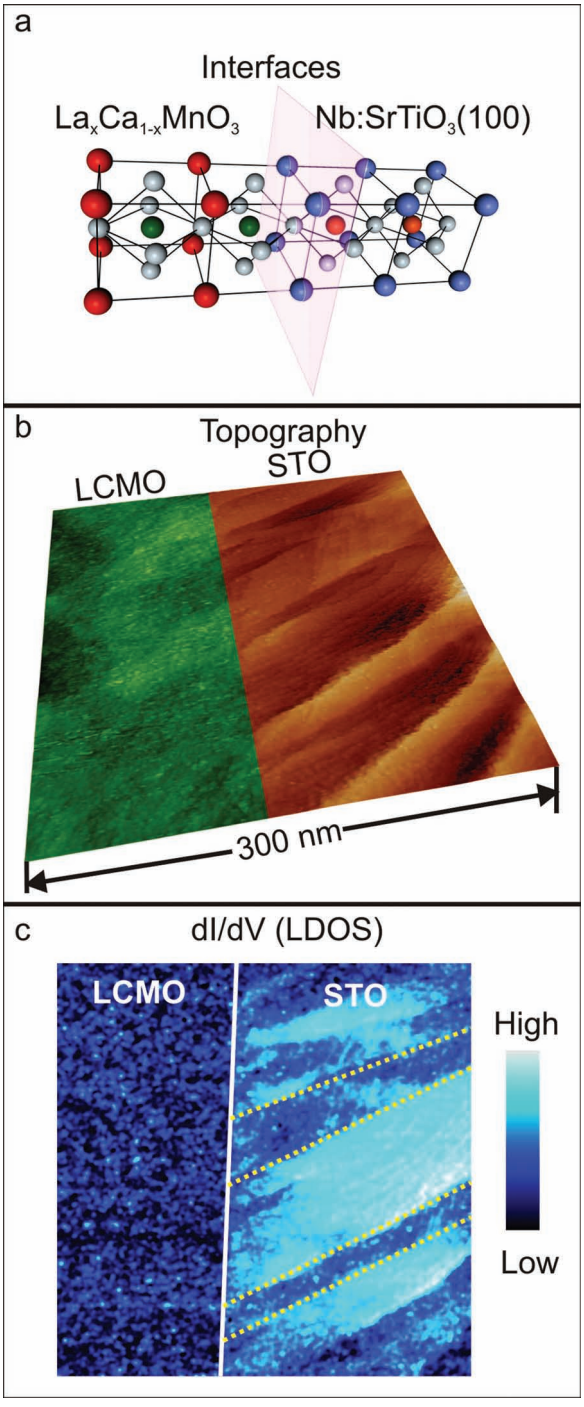

Figure 6. a) The schematic of the interface between $La_{2/3}Ca_{1/3}MnO_3$/Nb:$SrTiO_3$ (LCMO/Nb:STO). b) XSTM image at LCMO/Nb:STO interface. c) *dI/dV* contrast measured simultaneously as b).

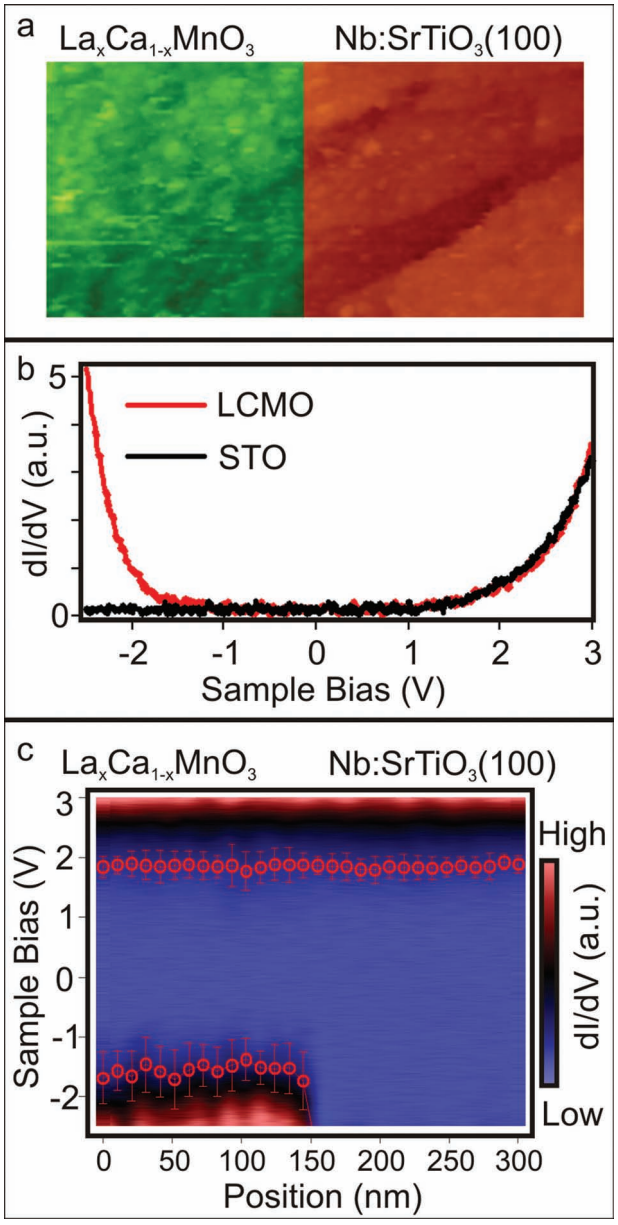

Figure 7. a) Zoom-in view of Figure 6b. b) *dI/dV* spectra measured at two different materials (LCMO and Nb:STO). c) Direct band mapping across LCMO/Nb:STO interfaces. This data is averaged from 30 × 30 grid spectra within 300 nm × 300 nm area.

terminated regions,[69] as shown in Figure 6c. In LCMO region, the surface does not exhibit clear terraces and steps. This is believed to be related to the strained nature of the LCMO film and/or the strain relaxation during the fracturing.[82]

From these images, it is clear that the *dI/dV* contrast at +3.0 V bias in LCMO region is similar to the TiO_2 terminated regions in Nb:STO (Figure 6c). The similar STS contrast (Figure 6c) can be understood from measured spectra on LCMO and on TiO_2 terminated Nb:STO regions. As shown in Figure 7b, the spectral weight is similar at positive bias resulting in little contrast between these regions (see Figure 6c). However, it is also clear that in the negative bias region, the spectral weight of LCMO is much higher than that of STO (either SrO or TiO_2 terminated surfaces) due to the smaller spacing to the valence band edge. With the ability to measure STS point by point, a 30 × 30 grid *dI/dV* spectra in a region near the interface with the scale of 300 nm x 300 nm were measured.[82] With this information, the averaged *dI/dV* spectra as function of the distance from the interface can be obtained and used to construct the electron band diagram across the interface (see Figure 7c). This clearly shows that the bands in LCMO and in Nb:STO are aligned for the unoccupied states (positive bias–conduction band), while the occupied states (negative bias) are not aligned. Using the well established formalism for semiconductor interfaces, previous studies that modeled the transport across single interface junctions had concluded that the conduction bands were not aligned.[83] This result clearly indicates that we need to re-examine the semiconductor formalism or the role of the STM measurement on the local band structure. Note that the absence of an observed band bending near the interface is due to the coarse spatial resolution (10 nm) and the expectation that the bands bend over a ~1 nm region near the interface.[82] This study highlights how XSTM/S can be utilized for studying interfaces in complex oxides heterostructures.

4.2. Nickelates: Schottky Barrier Revealed at $LaNiO_3$ - $Nb:SrTiO_3$ Interfaces

After demonstrating the ability to explore the manganite-titanate interface as shown above, we are now extending this work to explore the nature of other complex oxide-titanate interfaces. $LaNiO_3$ (LNO) is a metallic complex oxide at all temperature[84] and when it is grown on Nb:STO, which is an *n*-type material, a Schottky barrier is expected to form at the interfaces. **Figure 8**a shows the XSTM image of the fractured LNO/Nb:STO interface. The pillar-like morphology in LNO region is a result of strain relaxation in the 100 nm LNO film, which has been reported previously in relatively thick nickelate films.[85] It is intriguing to note that we observe a good correspondence between the microstructure in the bulk and the surface topography seen with the STM. A zoom-in view (left panel of Figure 8b) reveals an unexpected trench region at interface with ~7 nm wide near the interface. According to the STS measurements, this trench region is assigned to Nb:STO side of the interface. In STS mapping (Figure 8c), the trench region shows brighter contrast and then gradually decreases to bulk Nb:STO contrast when moving into Nb:STO region. While the detailed analysis is still in progress, the preliminary results suggest that this is due to the Schottky barrier formed due to interface charge transfer. The ~7 nm trench is consistent to the length scale of the band bending expected at this interface and calculated depletion region for the Schottky barrier. It is highly plausible that the built-in electric field in the band bending region alters the mechanical properties of Nb:STO and results in a physical trench during the fracturing process. This phenomenon is possible due to the strong electric field dependent permittivity of STO.[86] A dramatic change in permittivity indicates a large change in local electric dipoles, which are achieved by atomic movement within the unit cell. In short, this study illustrates how elastic properties can be altered by built-in electric field due to charge transfer at complex oxide interfaces at the nanoscale.

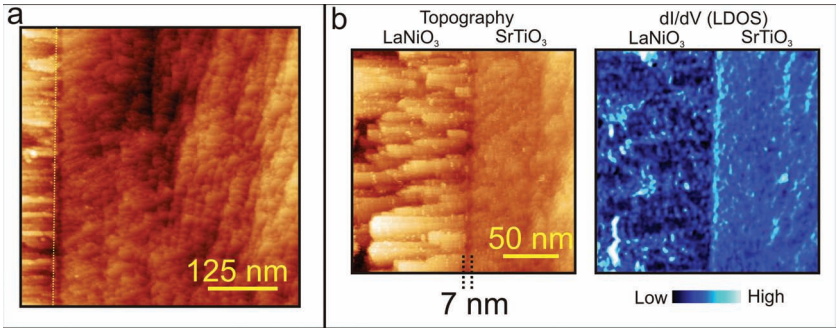

Figure 8. a) XSTM image of $LaNiO_3$/Nb:STO interfaces. b) Topography (left panel) and *dI/dV* contrast (right panel) recorded simultaneously. A ~7 nm wide trench (also shows a bright *dI/dV* contrast) was revealed at the interface.

4.3. Superlattices: $YBa_2Cu_3O_7/La_{2/3}Ca_{1/3}MnO_3$ Interfaces

After demonstrating the ability to image single interfaces, the extension of the technique requires expanding this approach to more complex architectures. As a prototypical test-case, we have recently applied XSTM to study $YBa_2Cu_3O_7/La_{2/3}Ca_{1/3}MnO_3$ (YBCO/LCMO) superlattices. The interplay between superconductivity and ferromagnetism has drawn plenty of attention due to the competing nature of the order parameters.[87] Cooper pairs in superconducting favor singlet spin coupling; while electrons in ferromagnetism favor same spin orientation. **Figure 9** shows the preliminary XSTM/S results that illustrates the capability of this approach to explore more complex architectures and the LDOS mapping will allow us to follow band evolution across multiple interfaces.

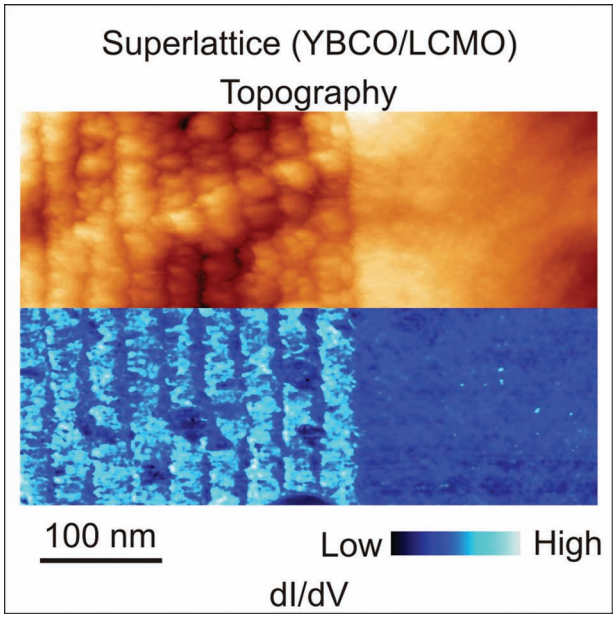

Figure 9. XSTM/S of $YBa_2Cu_3O_7/La_{2/3}Ca_{1/3}MnO_3$ (YBCO/LCMO) superlattice. Bright contrast in STS image represents the YBCO regions.

5. Summary and Perspectives

This article reviews the novel application of cross-sectional STM/S applied to complex oxide surfaces and interfaces developed at the Center for Nanoscale Materials at Argonne National Laboratory. Several fracturing procedures and issues have been discussed. This technique holds tremendous promise for future characterization of a wide range of oxide materials that do not have natural cleavage planes. With the increasing interests in the novel interfacial phenomena found at complex oxide interfaces, XSTM/S will provide unique information toward understanding the underlying physics.

Acknowledgements

Work at Argonne, including the Center for Nanoscale Materials, is supported by the U.S. Department of Energy, Office of Science, Office of Basic Energy Sciences, under Contract No. DE-AC02-06CH11357. J.C. was supported by DOD-ARO under the Grant No. 0402-17291 and NSF Grant No. DMR-0747808.

Received: November 21, 2012
Published online: March 26, 2013

[1] J. F. Zheng, X. Liu, N. Newman, E. R. Weber, D. F. Ogletree, M. Salmeron, *Phys. Rev. Lett.* **1994**, *72*, 1490.
[2] W. Melitz, J. Shen, S. Lee, J. S. Lee, A. C. Kummel, R. Droopad, E. T. Yu, *J. Appl. Phys.* **2010**, *108*, 023711.
[3] R. M. Feenstra, J. A. Stroscio, *J. Vac. Sci. Technol., B* **1987**, *5*, 923.
[4] R. M. Feenstra, D. A. Collings, D. Z. Y. Ting, M. W. Wang, T. C. McGill, *J. Vac. Sci. Technol., B* **1994**, *12*, 2592.
[5] R. M. Feenstra, J. A. Stroscio, J. Tersoff, A. P. Fein, *Phys. Rev. Lett.* **1987**, *58*, 1192.
[6] C. Celebi, J. K. Garleff, A. Y. Silov, A. M. Yakunin, P. M. Koenraad, *Phys. Rev. Lett.* **2010**, *104*, 086404.
[7] D. Kitchen, A. Richardella, J.-M. Tang, M. E. Flatté, A. Yazdani, *Nature* **2006**, *442*, 436.
[8] A. M. Yakunin, A. Y. Silov, P. M. Koenraad, J. H. Wolter, W. Van Roy, J. De Boeck, J.-M. Tang, M. E. Flatté, *Phys. Rev. Lett.* **2004**, *92*, 216806.
[9] A. M. Yakunin, A. Y. Silov, P. M. Koenraad, J.-M. Tang, M. E. Flatté, W. Van Roy, J. De Boeck, J. H. Wolter, *Phys. Rev. Lett.* **2005**, *95*, 256402.
[10] S. Gwo, K.-J. Chao, C. K. Shih, K. Sadra, B. G. Streetman, *Phys. Rev. Lett.* **1993**, *71*, 1883.
[11] O. Albrektsen, D. J. Arent, H. P. Meier, H. W. M. Salemink, *Appl. Phys. Lett.* **1990**, *57*, 31.
[12] R. M. Feenstra, D. A. Collins, D. Z. Y. Ting, M. W. Wang, T. C. McGill, *Phys. Rev. Lett.* **1994**, *72*, 2749.
[13] A. R. Smith, K.-J. Chao, C. K. Shih, Y. C. Shih, K. A. Anselm, B. G. Streetman, *J. Vac. Sci. Technol., B* **1995**, *13*, 1824.
[14] J. Harper, M. Weimer, D. Zhang, C.-H. Lin, S. S. Pei, *J. Vac. Sci. Technol., B* **1998**, *16*, 1389.
[15] R. M. Feenstra, *Physica B* **1999**, *273–274*, 796.
[16] J. Steinshnider, M. Weimer, R. Kaspi, G. W. Turner, *Phys. Rev. Lett.* **2000**, *85*, 2953.
[17] B. Z. Nosho, W. Barvosa-Carter, M. J. Yang, B. R. Bennett, L. J. Whitman, *Surf. Sci.* **2000**, *465*, 361.

[18] D. M. Bruls, J. W. A. M. Vugs, P. M. Koenraad, H. W. M. Salemink, J. H. Wolter, M. Hopkinson, M. S. Skolnick, F. Long, S. P. A. Gill, *Appl. Phys. Lett.* **2002**, *81*, 1708.
[19] S. L. Zuo, Y. G. Hong, E. T. Yu, J. F. Klem, *J. Appl. Phys.* **2002**, *92*, 3761.
[20] B. Z. Nosho, B. R. Bennett, L. J. Whitman, M. Goldenberg, *Appl. Phys. Lett.* **2002**, *81*, 4452.
[21] A. Mikkelsen, N. Skold, L. Ouattara, M. Borgstrom, J. N. Andersen, L. Samuelson, W. Seifert, E. Lundgren, *Nat. Mater.* **2004**, *3*, 519.
[22] A. Mikkelsen, N. Sköld, L. Ouattara, E. Lundgren, *Nanotechnology* **2006**, *17*, S362.
[23] A. Mikkelsen, E. Lundgren, *Prog. Surf. Sci.* **2005**, *80*, 1.
[24] K. M. Shen, J. C. S. Davis, *Mater. Today* **2008**, *11*, 14.
[25] M. Kugler, Ø. Fischer, C. Renner, S. Ono, Y. Ando, *Phys. Rev. Lett.* **2001**, *86*, 4911.
[26] M. Vershinin, S. Misra, S. Ono, Y. Abe, Y. Ando, A. Yazdani, *Science* **2004**, *303*, 1995.
[27] K. K. Gomes, A. N. Pasupathy, A. Pushp, S. Ono, Y. Ando, A. Yazdani, *Nature* **2007**, *447*, 569.
[28] S. H. Pan, E. W. Hudson, K. M. Lang, H. Eisaki, S. Uchida, J. C. Davis, *Nature* **2000**, *403*, 746.
[29] K. M. Lang, V. Madhavan, J. E. Hoffman, E. W. Hudson, H. Eisaki, S. Uchida, J. C. Davis, *Nature* **2002**, *415*, 412.
[30] J. E. Hoffman, E. W. Hudson, K. M. Lang, V. Madhavan, S. H. Pan, H. Eisaki, S. Uchida, J. C. Davis, *Science* **2002**, *295*, 466.
[31] E. W. Hudson, K. M. Lang, V. Madhavan, S. H. Pan, H. Eisaki, S. Uchida, J. C. Davis, *Nature* **2001**, *411*, 920.
[32] F. C. Niestemski, S. Kunwar, S. Zhou, S. Li, H. Ding, Z. Wang, P. Dai, V. Madhavan, *Nature* **2007**, *450*, 1058.
[33] J. Zhao, F. C. Niestemski, S. Kunwar, S. Li, P. Steffens, A. Hiess, H. J. Kang, S. D.Wilson, Z. Wang, P. Dai, V. Madhavan, *Nat. Phys.* **2011**, *7*, 719.
[34] S. Okamoto, A. J. Millis, *Nature* **2004**, *428*, 630.
[35] C. H. Ahn, K. M. Rabe, J.-M. Triscone, *Science* **2004**, *303*, 488.
[36] P. Zubko, S. Gariglio, M. Gabay, P. Ghosez, J.-M. Triscone, *Annu. Rev. Condens. Matter Phys.* **2011**, *2*, 141.
[37] A. P. Ramirez, *J. Phys.: Condens. Matter.* **1997**, *9*, 8171.
[38] J. Orenstein, A. J. Mills, *Science* **2000**, *288*, 468.
[39] T. Tybell, C. H. Ahn, J.-M. Triscone, *Appl. Phys. Lett.* **1999**, *75*, 856.
[40] D. D. Fong, G. B. Stephenson, S. K. Streiffer, J. A. Eastman, O. Auciello, P. H. Fuoss, C. Thompson, *Science* **2004**, *304*, 1650.
[41] N. Yanase, K. Abe, N. Fukushima, T. Kawakubo, *Jpn. J. Appl. Phys.* **1999**, *38*, 5305.
[42] R. Ramesh, N. A. Spaldin, *Nat. Mater.* **2007**, *6*, 21.
[43] G. Binnig, H. Rohrer, Ch. Gerber, E. Weibel, *Phys. Rev. Lett.* **1983**, *50*, 120.
[44] R. G. Moore, J. Zhang, V. B. Nascimento, R. Jin, J. Guo, G. T. Wang, Z. Fang, D. Mandrus, E. W. Plummer, *Science* **2007**, *318*, 615.
[45] S. S. P. Parkin, R. Sigsbee, R. Felici, G. P. Felcher, *Appl. Phys. Lett.* **1986**, *48*, 604.
[46] V. B. Nascimento, J. W. Freeland, R. Saniz, R. G. Moore, D. Mazur, H. Liu, M. H. Pan, J. Rundgren, K. E. Gray, R. A. Rosenberg, H. Zheng, J. F. Mitchell, A. J. Freeman, K. Veltruska, E. W. Plummer, *Phys. Rev. Lett.* **2009**, *103*, 227201.
[47] G. van der Laan, M. A. Hoyland, M. Surman, C. F. J. Flipse, B. T. Thole, *Phys. Rev. Lett.* **1992**, *69*, 3827.
[48] J. Chakhalian, J. W. Freeland, G. Srajer, J. Strempfer, G. Khaliullin, J. C. Cezar, T. Charlton, R. Dalgliesh, C. Bernhard, G. Cristiani, H.-U. Habermeier, B. Keimer, *Nat. Phys.* **2006**, *2*, 244.
[49] N. Nakagawa, H. Y. Hwang, D. A. Muller, *Nat. Mater.* **2006**, *5*, 204.
[50] J. Chakhalian, J. W. Freeland, H.-U. Habermeier, G. Cristiani, G. Khaliullin, M. van Veenendaal, B. Keimer, *Science* **2007**, *318*, 1114.
[51] The whole issue 11 in volume 33 of *MRS Bulletin* (2008) was devoted to the "whither oxide electronics?"; The "Focus" of No. 2, Volume 11 of *Nature Materials* (2012) was devoted to the "oxide interfaces".
[52] R. Ramesh, D. G. Schlom, *MRS Bull.* **2008**, *33*, 1006.
[53] J. Chakhalian, A. J. Millis, J. Rondinelli, *Nat. Mater.* **2012**, *11*, 92.
[54] M. Bibes, J. E. Villegas, A. Barthelemy, *Adv. Mater.* **2011**, *60*, 5.
[55] A. Ohtomo, H. Y. Hwang, *Nature* **2004**, *427*, 423.
[56] N. Reyren, S. Thiel, A. D. Caviglia, L. F. Kourkoutis, G. Hammerl, C. Richter, C. W. Schneider, T. Kopp, A.-S. Ruetschi, D. Jaccard, M. Gabay, D. A. Muller, J.-M. Triscone, J. Mannhart, *Science* **2007**, *317*, 1196.
[57] A. Gozar, G. Logvenov, L. F. Kourkoutis, A. T. Bollinger, L. A. Giannuzzi, D. A. Muller, I. Bozovic, *Nature* **2008**, *455*, 782.
[58] K. Ueda, H. Tabata, T. Kawai, *Science* **1998**, *280*, 1064.
[59] K. S. Takahashi, M. Kawasaki, Y. Tokura, *Appl. Phys. Lett.* **2001**, *79*, 1324.
[60] P. Padhan, W. Prellier, R. C. Budhani, *Appl. Phys. Lett.* **2006**, *88*, 192509.
[61] H. Zheng, F. Straub, Q. Zhan, P.-L. Yang, W.-K. Hsieh, F. Zavaliche, Y.-H. Chu, U. Dahmen, R. Ramesh, *Adv. Mater.* **2006**, *18*, 2747.
[62] D. A. Muller, L. Fitting Kourkoutis, M. Murfitt, J. H. Song, H. Y. Hwang, J. Silcox, N. Dellby, O. L. Krivanek, *Science* **2008**, *319*, 1073.
[63] Z. Wang, F. Yang, Z. Zhang, Y. Tang, J. Feng, K. Wu, Q. Guo, J. Guo, *Phys. Rev. B* **2011**, *83*, 155453.
[64] D. A. Bonnell, *Prog. Surf. Sci.* **1998**, *57*, 187.
[65] D. A. Bonnell, J. Garra, *Rep. Prog. Phys.* **2008**, *71*, 044501.
[66] C. Cen, S. Thiel, G. Hammerl, C. W. Schneider, K. E. Andersen, C. S. Hellberg, J. Mannhart, J. Levy, *Nat. Mater.* **2008**, *7*, 298.
[67] M. Basletic, J.-L. Maurice, C. Carrétéro, G. Herranz, O. Copie, M. Bibes, É. Jacquet, K. Bouzehouane, S. Fusil, A. Barthélémy, *Nat. Mater.* **2008**, *7*, 621.
[68] T. Y. Chien, N. P. Guisinger, J. W. Freeland, *J. Vac. Sci. Technol., B* **2010**, *28*, C5A11.
[69] N. P. Guisinger, T. S. Santos, J. R. Guest, T. Y. Chien, A. Bhattacharya, J. W. Freeland, M. Bode, *ACS Nano* **2009**, *3*, 4132.
[70] T. Y. Chien, N. P. Guisinger, J. W. Freeland, *Proc. SPIE* **2011**, *7940*, 79400T.
[71] Y. Pennec, N. J. C. Ingle, I. S Elfimov, E. Varene, Y. Maeno, A. Damascelli, J. V. Barth, *Phys. Rev. Lett.* **2008**, *101*, 216103.
[72] B. Bryant, Ch. Renner, Y. Tokunaga, Y. Tokura, G. Aeppli, *Nat. Commun.* **2011**, *2*, 212.
[73] A. R. Schmidt, K. Fujita, E.-A. Kim, M. J. Lawler, H. Eisaki, S. Uchida, D.-H. Lee, J. C. Davis, *New J. Phys.* **2011**, *13*, 065014.
[74] A. F. Santander-Syro, O. Copie, T. Kondo, F. Fortuna, S. Paihés, R. Weht, X. G. Qiu, F. Bertran, A. Nicolaou, A. Taleb-Ibrahimi, P. Le Févre, G. Herranz, M. Bibes, N. Reyren, Y. Aperter, P. Lecoeur, A. Barthélémy, M. J. Rozenberg, *Nature* **2011**, *469*, 189.
[75] W. Meevasana, P. D. C. King, R. H. He, S.-K. Mo, M. Hashimoto, A. Tamai, P. Songsiriritthigul, F. Baumberger, Z.-X. Shen, *Nat. Mater.* **2011**, *10*, 114.
[76] T. Y. Chien, T. S. Santos, M. Bode, N. P. Guisinger, J. W. Freeland, *Appl. Phys. Lett.* **2009**, *95*, 163107.
[77] S. P. McJunkins, J. I. Thornton, *Forensic Sci.* **1973**, *2*, 1.
[78] B. Reihl, J. G. Bednorz, K. A. Müller, Y. Jugnet, G. Landgren, J. F. Morar, *Phys. Rev. B* **1984**, *30*, 803.
[79] S. Kohiko, M. Arai, H. Yoshikawa, S. Fukushima, M. Oku, Y. Waseda, *Phys. Rev. B* **2000**, *62*, 7964.
[80] T. Y. Chien, J. W. Freeland, N. P. Guisinger, *Appl. Phys. Lett.* **2012**, *100*, 031601.

[81] F. W. Lytle, *J. Appl. Phys.* **1964**, *35*, 2212.
[82] T. Y. Chien, J. Liu, J. Chakhalian, N. P. Guisinger, J. W. Freeland, *Phys. Rev. B* **2010**, *82*, 041101(R).
[83] W. M. Lü, J. R. Sun, D. J. Wang, Y. W. Xie, S. Liang, Y. Z. Chen, B. G. Shen, *Appl. Phys. Lett.* **2008**, *92*, 062503.
[84] J. B. Torrance, P. Lacorre, A. I. Nazzal, E. J. Ansaldo, Ch. Niedermayer, *Phys. Rev. B* **1992**, *45*, 8209.
[85] M. A. Novojilov, O. Yu. Gorbenko, I. E. Graboy, A. R. Kaul, H. W. Zandbergen, N. A. Babushkina, L. M. Belova, *App. Phys. Lett.* **2000**, *76*, 2041.
[86] H.-M. Christen, J. Mannhart, E. J. Williams, Ch. Gerber, *Phys. Rev. B* **1994**, *49*, 12095.
[87] A. M. Goldman, V. Vas'ko, P. Kraus, K. Nikolaev, V. A. Larkin, *J. Mag. Mag. Mater.* **1999**, *200*, 69.